Symbolic-regression aided development of a new cubic equation of state for improved liquid phase density calculation at pressures up to 100 MPa

Xiaoxian Yang

xiaoxian.yang@mb.tu-chmenitz.de

Chemnitz University of Technology

Ophelia Frotscher

Chemnitz University of Technology

Markus Richter

Chemnitz University of Technology

Research Article

Keywords: cubic equation of state, liquid density, machine learning, symbolic regression

Posted Date: December 12th, 2024

DOI: https://doi.org/10.21203/rs.3.rs-5447725/v1

Additional Declarations: No competing interests reported.

Version of Record: A version of this preprint was published at International Journal of Thermophysics on January 27th, 2025. See the published version at https://doi.org/10.1007/s10765-024-03490-5.

Symbolic-regression aided development of a new cubic equation of state for improved liquid phase density calculation at pressures up to 100 MPa

Xiaoxian Yang*, Ophelia Frotscher, Markus Richter†

Chemnitz University of Technology, Applied Thermodynamics, 09107 Chemnitz, Germany

Abstract

For over a century, cubic equations of state (EoS) have been used to calculate density and phase equilibria of pure fluids and mixtures. Despite a century's development with hundreds of resulting cubic EoS, their accuracy in liquid phase density calculations is still unsatisfactory. In this work, a new cubic EoS was developed to improve the accuracy of liquid phase density calculation while keeping similar accuracy of other properties. The new cubic EoS, named YFR (Yang-Frotscher-Richter) EoS, was developed based on the functional form of the Patel-Teja (PT) EoS [$p = RT/(v-b) - a/(v(v+b)+c(v-b)]$. In the PT EoS, parameters b and c are linked to an empirical critical compressibility factor ξ_C, and all these three parameters are constants for a pure fluid. By contrast, in the YFR EoS, ξ_C, b, and c are functions of temperature, and the equations describing this dependency were developed with symbolic regression. This is the key to improving liquid phase density calculation, although it leads to thermodynamic inconsistencies at high pressures. The application range of the new cubic EoS is thus limited to pressures up to 100 MPa. The YFR EoS was developed using nearly all pure fluids available in NIST's REFPROP 10.0 database, with reference values computed with REFPROP. The average of the absolute value of relative deviations (AARD) of liquid phase densities calculated with the YFR EoS from reference values is approximately 2%, compared to 3% when using the Patel-Teja-Valderrama (PTV) EoS and 6% when using the Peng-Robinson (PR) EoS. The YFR EoS has been implemented in our self-developed OilMixProp 1.0 software package.

Keywords: cubic equation of state, liquid density, machine learning, symbolic regression

---

* Corresponding author. Tel.: +49 371 531-36921. Email address: xiaoxian.yang@mb.tu-chmenitz.de.
ORCID ID: https://orcid.org/0000-0003-4655-3156.

† Corresponding author. Tel.: +49 371 531-38050. Email address: m.richter@mb.tu-chmenitz.de.
ORCID ID: https://orcid.org/0000-0001-8120-5646.

1. Introduction

For over a century, cubic equations of state (EoS) have been used for the calculation of density, phase equilibria (mainly vapor-liquid-equilibrium, VLE), and residual properties (e.g., residual entropy) of pure fluids and mixtures. They strike a reasonable balance of simplicity, accuracy, and generality and thus are commonly used in industry. Reviews of cubic EoS are available in literature covering various aspects, e.g., equation form [1], α-function [2], binary interaction parameter for mixtures [3], or a unique group of EoS [4]. Despite the developments over a century and the hundreds of resulting equations available, the accuracy of liquid phase density calculation using a cubic EoS is still unsatisfactory, and this has already been recognized for a long time [5]. Efforts from scientists and industries have been devoted to improving the situation, but very slowly. On the one hand, there have been excellent alternatives, e.g., highly accurate multi-parameter EoS available in virtually free software (such as REFPROP 10.0 [6], TREND 5.0 [7] , and CoolProp 6.4.1 [8]). On the other hand, developing a new cubic EoS with improved performance over all others is very challenging: A cubic EoS, fundamentally a 3-order power function, is limited by its simple form and subject to many constraints (e.g., those at the critical point [9]), while it is expected to work for a large variety of fluids (from light gases to dense fluids) with descent accuracy for all calculable properties. Nonetheless, the industry favors cubic EoS as they are easily programmed and computationally cost-effective. Any improvement in the cubic EoS could significantly benefit the industry. In this work, we developed a new general cubic EoS aided with symbolic regression (SR) to improve the accuracy of liquid phase density while keeping the accuracy of other properties at pressures below 100 MPa (typical range of industrial applications). For convenience of description, the new EoS will be named YFR (Yang-Frotscher-Richter) EoS.

The present work was also motivated by one of our previous studies [10,11], in which a novel model approach was developed to calculate all the core thermophysical properties (density, phase equilibria, heat capacity, entropy, enthalpy, speed of sound, viscosity, and thermal conductivity) of oils. This modeling approach can be easily extended to mixtures, e.g., oil + refrigerant mixtures. Here, a cubic EoS is needed for the calculation of the density and phase equilibria; with an additional equation for the ideal gas isobaric heat capacity c_{p}^{0}, the caloric properties can be obtained and, by adopting the state-of-the-art residual entropy scaling (RES) methods developed by Yang et al. [12–17], viscosity and thermal conductivity can be calculated. In this approach, the cubic EoS

was also needed to fit the acentric factor ω (an important constant of a pure fluid) of the quasi-pure oil. Six cubic EoS were studied, including Soave-Redlich-Kwong (SRK) [18], Peng-Robinson (PR) [19], Peng-Robinson-Stryjek-Vera (PRSV) [20], Wilson-Redlich-Kwong (WRK) [21], Patel-Teja-Valderrama (PTV) [22] and Redlich-Kwong (RK) [23]. As a result, only the PTV EoS, which is based on the Patel-Teja (PT) EoS [9], produced reasonable values of ω because it can calculate the liquid density more accurately than others [4]. Using this oil modeling approach, calculations generally agree with the experimental data within the same level of experimental uncertainty for most of the properties, except for density and viscosity. Therefore, a new cubic EoS with overall better performance than the PTV EoS is needed to further improve this approach in density calculation.

As will be discussed in more details in Sections 2 and 3, the new cubic EoS would be developed in the form of a generalized three-parameter cubic EoS first proposed by Patel and Teja [9]:

$$p = \frac{RT}{v-b} - \frac{a}{v^2 + (b+c)v - bc} \tag{1}$$

Here p, T, and v are pressure, temperature, and molar volume respectively, R = 8.3144598 J·K^{-1}·mol^{-1} is the gas constant. In the PT EoS [9], parameters b and c are related to an empirical critical compressibility factor ξ_C, and all these three parameters are constants for a pure fluid. The key innovation in this work is to make ξ_C, b, and c dependent on temperature while the corresponding equation forms are developed with SR. This improves the accuracy of the liquid phase density calculation. However, it results in thermodynamic inconsistency at high pressures, mainly because parameter b is temperature-dependent [24–27]. A comprehensive study of thermodynamic inconsistency will be presented in Section 4.3. As a result, the new cubic EoS is still very reliable at pressures below 100 MPa, which becomes the application range of the new cubic EoS. Most industrial applications, especially those involving oils and refrigerants, are within this range, except for some applications in rheology [28] and tribology [29].

Symbolic regression (SR) is a supervised machine learning approach that searches for the simplest combination of pre-selected mathematical expressions that best fits given data sets. In our previous work, a thermodynamics-informed symbolic regression (TiSR) tool [30] was developed, which aims at thermodynamic equation developments using SR. It has been successfully combined with data acquisition and optimal experimental design (OED) to form an integrated experimental-

computational approach for the development of thermodynamic equations, as previously described by us [31–33]. An important factor for 'thermodynamics-informed' SR is to add constants (e.g., critical point), as done by Sekulla et al.[34], and constraints (e.g., those at the critical point [9]) to the equation development, which was discussed in detail in our previous work [30,35]. (TiSR is publicly available at https://github.com/scoop-group/TiSR.) In this work, TiSR and another publicly available SR tool, GPTIPS2F (https://github.com/is-centre/gptips2f-matlab), were adopted to develop the YFR EoS. GPTIPS2F was developed earlier than TiSR by Dr. Dominic Searson and, since 2017, maintained by Dr. Aleksei Tepljakov, TalTech University. We used two SR tools hoping to obtain as many good candidate equations as possible, nevertheless, both tools eventually produce almost the same results of the good equations.

In this work, we will present the final YFR EoS equation in Section 2. Development details are given in Section 3, and the evaluation of this new cubic EoS is shown in Section 4. Part of this effort is funded by KETEC (Research Platform for Refrigeration and Energy Technology) [36].

2. The YFR EoS

The YFR EoS, applicable at pressures below 100 MPa, adopts the form of a generalized three-parameter cubic EoS as given in Eq. (1). Parameters a, b, and c in Eq. (1) are:

$$a = \alpha \cdot \Omega_a \frac{R^2 T_c^2}{p_c} \tag{2}$$

$$b = \Omega_b \frac{R T_c}{p_c} \tag{3}$$

$$c = \Omega_c \frac{R T_c}{p_c} \tag{4}$$

Here, T_c and p_c are critical temperature and critical pressure, respectively. The function α as well as the parameters Ω_a, Ω_b and Ω_c can be specifically formulated to produce most of the existing cubic EoS [37]. For the YFR EoS, they are as follows:

$$\alpha = (1 + m \cdot (1 - T_r^{0.5}))^2 \tag{5}$$

$$m = n_{m,1} \cdot Z_c + n_{m,2} \cdot \omega Z_c + n_{m,3} \tag{6}$$

$$X = n_{X,1} \cdot \exp(-T_r^4) + n_{X,2} \cdot \exp(-T_r^3) + n_{X,3} \cdot Z_c + n_{X,4}, (X = \Omega_a, \Omega_b \text{ and } \xi_c) \quad (7)$$

$$\Omega_c = 1 - 3\xi_c \quad (8)$$

$$dX/dT = 0, (X = \Omega_a, \Omega_b, \Omega_c \text{ and } \xi_c) \quad (9)$$

Here, $T_r = T/T_c$ is the reduced temperature, ω is acentric factor, ξ_c is an empirical critical compressibility factor different from the experimental one Z_c. The functional forms of Eqs. (6) and (7) were obtained with our SR tool TiSR, and the parameters, as listed in Table 1, were determined with a nonlinear regression (NR) tool. For mixtures, the van der Waals mixing rule was used as by PTV EoS in our previous work [10].

Table 1: Parameters of the YFR EoS

	$i = 1$	$i = 2$	$i = 3$	$i = 4$
$n_{m,i}$	2.779200	5.208803	−0.314477	
$n_{\Omega a,i}$	−0.174696	0.156625	−1.158565	0.784751
$n_{\Omega b,i}$	0.048371	−0.043334	0.319103	−0.012341
$n_{\xi c,i}$	0.144894	−0.129835	0.957454	0.036884

In the YFR EoS, the parameters Ω_a, Ω_b, and Ω_c are functions of temperature for a pure fluid, while they are constants in most other cubic EoS. This is the key to improving the accuracy of the liquid phase density while keeping the accuracy of other parameters at pressures below 100 MPa. However, this increases the complexity of the EoS, especially for those terms involving temperature derivatives (e.g., residual entropy, see the appendix), and results in thermodynamic inconsistency, mainly due to the fact that the parameters Ω_b and b are temperature dependent [24–27].

As will be discussed in Section 4.3, the temperature dependence of Ω_a, Ω_b, and Ω_c makes calculations of the YFR EoS deviate at high pressures (e.g., p > 50 MPa) from the reference values and most other reliable cubic EoS. To fix this problem, Eq. (9) is introduced (see detailed discussion in Section 4.3.1), that is, the temperature derivatives of Ω_a, Ω_b, and Ω_c of this semi-empirical cubic EoS are set to zero. This brings inconsistence to the YFR EoS itself, but it yields other benefits: (1) the negative value of the heat capacity at high pressures (one of the characteristics of thermodynamic inconsistence [24–27]) is avoided; see Section 4.3.2, and (2) to an existing computational code for a generalized three-parameter cubic EoS, only a few changes are needed to implement the YFR EoS. However, Eq. (9) cannot resolve the issue that

the isotherms in the pressure-volume phase diagram cross each other at high pressures (another characteristic of thermodynamic inconsistence [24–27]), see Section 4.3.2. Therefore, the application range of this new cubic EoS is limited to pressures below 100 MPa. The YFR EoS has been implemented in our OilMixProp 1.0 software package [38].

3. EoS Development

3.1 Overview

In this subsection, we provide details on how the YFR EoS was developed. The used generalized three-parameter cubic EoS was first proposed by Patel and Teja [9], who also proposed an empirical critical compressibility factor

$$\xi_{\mathrm{c}} = \frac{p_{\mathrm{c}} v_{\mathrm{c}}}{R T_{\mathrm{c}}} \tag{10}$$

Here, v_{c} is the molar volume at the critical point. Together with the constraints [9] at the critical point,

$$\left(\frac{\partial p}{\partial v}\right)_{T_{\mathrm{c}}} = 0 \tag{11}$$

$$\left(\frac{\partial^2 p}{\partial v^2}\right)_{T_{\mathrm{c}}} = 0 \tag{12}$$

Eqs. (1) to (4), can be reformulated to yield Ω_a, Ω_b and Ω_c as functions of ξ_{c}

$$\Omega_a = 3{\xi_{\mathrm{c}}}^2 + 3(1 - 2\xi_{\mathrm{c}})\Omega_b + {\Omega_b}^2 + 1 - 3\xi_{\mathrm{c}} \tag{13}$$

Ω_b being the smallest positive root of

$${\Omega_b}^3 + (2 - 3\xi_{\mathrm{c}}){\Omega_b}^2 + 3{\xi_{\mathrm{c}}}^2\Omega_b - {\xi_{\mathrm{c}}}^3 = 0 \tag{14}$$

and Ω_c according to Eq. (8).

With Eq. (1) to (4), (8), (13) and (14) combined, it is easy to see that, given T and v, p can be calculated if α and ξ_{c} are known. On the contrary, if accurate (p, v, T) data are available, for example, from reliable experiments or reference EoS, α and ξ_{c} at can be fitted. Mathematically, α and ξ_{c} could be functions of both T and v (or p); nevertheless, for simplicity, we only

considered α and ξ_c as functions of T. The flow chart to determine $\alpha(T)$ and $\xi_c(T)$ is depicted in Figure 1, and details are described in the following subsections.

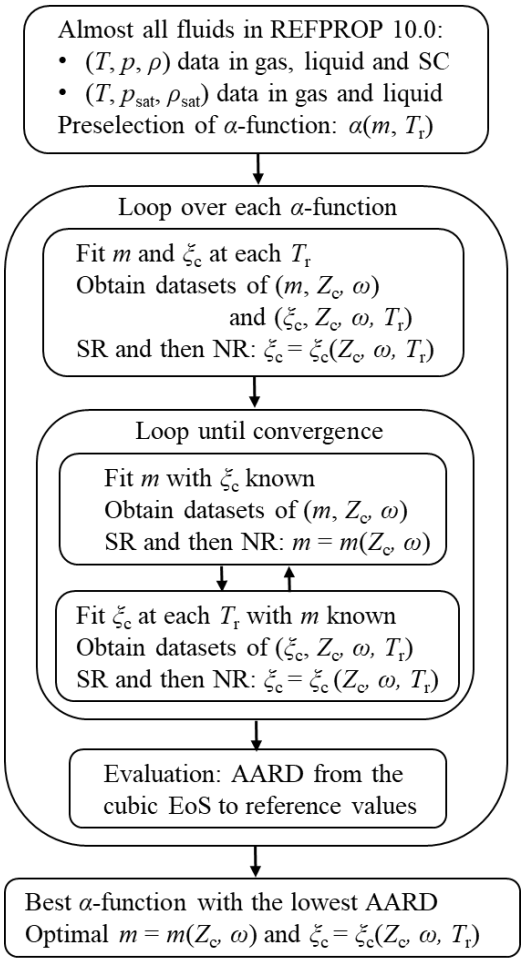

Figure 1. The flow chart to determine $\alpha(T)$ and $\xi_c(T)$. SC: supercritical region. SR: symbolic regression. NR: non-linear regression. The subscript 'sat' refers to saturation conditions.

3.2 Reference Values

First, rather than experimental data, REFPROP 10.0 calculations were used as reference values. On the one hand, the reference EoS implemented in REFPROP 10.0 are highly accurate and are often used to compare new experimental data. On the other hand, it saves lots of time and effort in collecting and evaluating the experimental data (e.g., removing those with very high uncertainty). To develop a general EoS suitable for a wide variety of fluids (light gaseous fluids

to dense fluids), almost all the fluids in REFPROP 10.0 were adopted. Very little data, for example, from ethylene oxide, led to initial-value problems within the iteration (see Figure 1). Therefore, instead of using these data for fitting, we used these data to check the extrapolation behavior of the new EoS.

In the subcritical region, from triple-point temperature to $0.95 \cdot T_c$, (T, p, ρ) data in the homogeneous phases and (T, p_{sat}, ρ_{sat}) data at saturation conditions were calculated with REFPROP 10.0. These data were used to fit $\alpha(T)$, $\xi_c(T)$, or both simultaneously at each temperature. In the supercritical region, (T, p, ρ) data up to $5.0\,T_c$ and $5.0\,p_c$ (or the limits of REFPROP 10.0) were calculated to fit $\alpha(T)$ and $\xi_c(T)$ in this region. With $\alpha(T)$ and $\xi_c(T)$ at each temperature T in the subcritical and supercritical regions fitted, the SR tools were used to determine the best functional form of $\alpha(T)$ and $\xi_c(T)$, and a NR tool (function *lsqcurvefit* in Matlab) was used to determine the parameters, as discussed below.

3.3 α-function

The function $\alpha(T)$ is subject to many constraints (see [2]). These constraints limit the form of $\alpha(T)$ to a few types. The GPTIPS2F tool does not consider these thermodynamic constraints, and these constraints are not yet implemented in our TiSR tool. Therefore, a few preselections based on Table 2 of Valderrama [1] were adopted, and the following two are among the best candidates:

$$\alpha = \exp(m \cdot (1 - T_r^n)) \tag{15}$$

$$\alpha = (1 + m \cdot (1 - T_r^n))^2 \tag{16}$$

In Eqs. (15) and (16), m and n are expected to be constants for each pure fluid. Although Eq. (16) does not perfectly meets all the constraints of $\alpha(T)$ function (see [2]), while Eq. (15) does, the result showed that Eq. (16) is better for the calculations in the subcritical region. This agrees with the finding of Patel and Teja [9]. Furthermore, in Eq. (16), although an optimal n was found in the range of 0.4 ~ 0.6 in the optimization loop, fixing it to 0.5 did not yield an obviously worse result. To reduce the complexity of the YFR EoS, n in Eq. (16) was eventually set to 0.5, and this yielded Eq. (5).

With a pre-selected $\alpha(m, T_r)$ function, the fitting of m and ξ_c (simultaneously or separately) at each temperature could be carried out. Two data sets (m, Z_c, ω) and (ξ_c, Z_c, ω, T_r) of approximately 140 fluids from the triple-point temperature to $5.0 \cdot T_c$ (or the limits of REFPROP 10.0) were collected. SR was carried out to obtain the best possible functional forms for $m = m(Z_c, \omega)$ and $\xi_c = \xi_c(Z_c, \omega, T_r)$, and the parameters in these equations were fitted with *lsqcurvefit* , which is a solver in *Matlab* for non-linear least squares problems. As a result, Eq. (6) was found to be one of the best equations for $m = m(Z_c, \omega)$. The determination of the equation $\xi_c = \xi_c(Z_c, \omega, T_r)$ took more effort and is discussed in more details in the following subsection.

3.4 ξ_c-function

Both SR tools used delivered a series of equations in the Pareto front of complexity of the equation vs. accuracy of the fitting. As expected, with more terms and parameters, the equations can fit the data better. Equations with four terms already achieved good accuracy, and more terms did not yield a significant improvement. As a result, Eq. (7) is among the best candidates for $\xi_c = \xi_c(Z_c, \omega, T_r)$. Other best candidates are those similar to Eq. (7) but with the second term replaced by Z_c/T_r, $Z_c^{T_r^2}$, or $1/T_r \cdot \exp(-Z_c)$, or with the third term replaced by $Z_c^{Z_c}$. Finally, with the optimal parameters determined by the NR tool, Eq. (7) stands out, yielding almost the best agreement with the data. The agreement is characterized by the root mean square (RMS) of the relative deviations from the data to the equation. Here, 'almost' is used because the agreement is the best if the third term was replaced by $Z_c^{Z_c}$. However, Eq. (7) was chosen because the term $Z_c^{Z_c}$ is a bit more complicated while the improvement is negligibly small. Furthermore, when using both SR tools, ω only occurred in the equations when more than four terms were used. This leads to the assumption that ω has no impact on ξ_c, which is why $\xi_c = \xi_c(Z_c, \omega, T_r)$ was simplified to $\xi_c = \xi_c(Z_c, T_r)$.

The empirical critical compressibility factor ξ_c fitted against calculations of REFPROP 10.0, namely optimal-ξ_c, and the correlation of $\xi_c = \xi_c(Z_c, T_r)$ are plotted in Figure 2 for six exemplar pure fluids. These fluids include: three light to heavy hydrocarbons (methane, pentane, and hexadecane, i.e., C16), a refrigerant (R134a) and two fluids (Xenon and SF_6) with unique optimal-ξ_c shapes. The data trends of optimal-ξ_c vs. T_r (red circles in Figure 2) more or less decrease in the low T_r range ($T_r < 1.5$) and increase in the high T_r range ($T_r > 1.5$), while the

exact shapes differ between fluids, especially in the high T_r range. The correlation (black curve in Figure 2) can generally agree with the optimal-ξ_C in the low T_r range, while it tends to be a constant in the high T_r range to cope with variations between fluids. One could expect that if unique parameters of Eq. (7) are fitted for each pure fluid, the agreement between the optimal-ξ_c and the correlation will be better, and thus the YFR EoS will yield better performance. This opens the door for further future improvements of such cubic EoS.

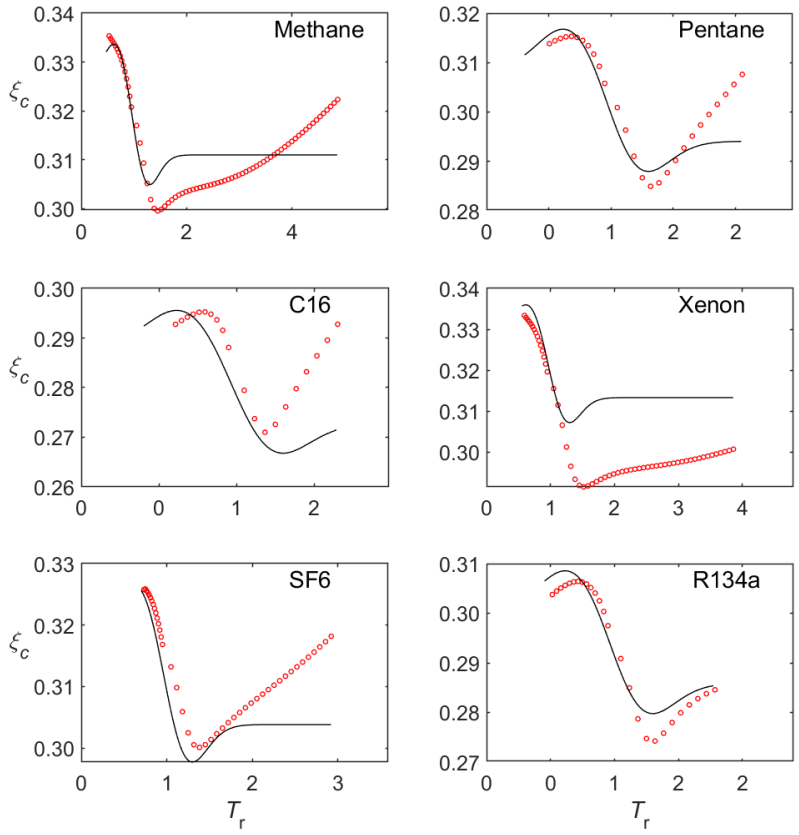

Figure 2. Empirical critical compressibility factor ξ_c plotted versus reduced temperature $T_r = T/T_c$ for six selected pure fluids. Red circle: optimal value fitted against the calculations of REFPROP 10.0, solid curves: calculations with Eq. (7).

At last, with $\xi_c = \xi_c(Z_c, T_r)$ determined, Ω_a, Ω_b and Ω_c can be calculated using Eqs. (8), (13) and (14). Alternatively, considering that solving Eq. (14) is an additional burden on the computer and is not favored by users, the equations and parameters for each of the Ω_a, Ω_b and Ω_c were fitted to the same form as for ξ_c, see Eqs. (7) and (8).

4. Evaluations and Discussions

The YFR EoS has been implemented in our OilMixProp 1.0 software package [38]. Here, the evaluation in calculating densities (T, p, ρ) and phase behaviors (T, p_{sat}, ρ_{sat}) of pure fluids will be presented first. Later, with an additional equation for ideal gas isobaric heat capacity as a function of temperature, $c_p^0(T)$, the calculation of caloric properties will be evaluated. Calculations of transport properties (viscosity and thermal conductivity) are a bit more complicated, and an evaluation of these properties will be presented in our future work. The thermodynamic inconsistency is then studied, and limitations are provided. Finally, the YFR EoS was applied to oil density calculations, yielding better results than the PTV EoS used in our previous work [10].

4.1 Density and Phase Behavior

The average of the absolute value of relative deviations (AARD) of properties calculated with PR, SRK, PTV and YFR EoS from the reference values (calculated with REFPROP 10.0) is shown in Figure 3. The calculated properties include pressure p_{sat}, vapor density $\rho_{sat,vap}$, and liquid density $\rho_{sat,liq}$ at saturation conditions, as well as densities (ρ_{vap}, ρ_{liq}, and ρ_{SC}) in the homogeneous vapor phase and liquid phases as well as in the supercritical region. All fluids implemented in REFPROP 10.0 were calculated from triple point to $5.0 \cdot T_c$ and $5.0 \cdot p_c$ (or the limits of REFPROP 10.0). According to Figure 3, for the six properties, among the four EoS, the YFR EoS is either the best one or among the best two. When the YFR EoS is not the best one, it is only slightly worse than the best one. In particular, with the YFR EoS, the AARD are all less than 3.0%, except for $\rho_{sat,vap}$ reaching 3.4%. Furthermore, the AARD for the saturated liquid density is 2.5% and for the homogeneous liquid density is 2.0%, which are obviously better than other EoS.

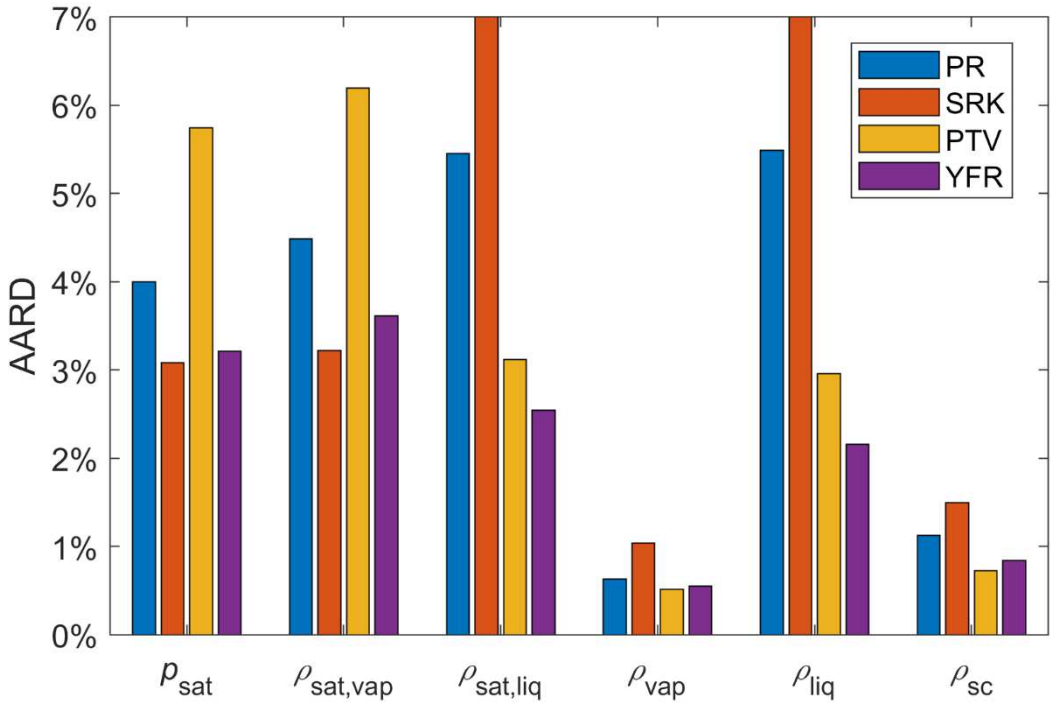

Figure 3. The average of the absolute value of relative deviations (AARD) of properties calculated with PR, SRK, PTV, and YFR EoS from reference values (calculated with REFPROP 10.0). The properties are pressure p_{sat}, vapor density $\rho_{sat,vap}$, and liquid density $\rho_{sat,liq}$ at saturation conditions, and densities ρ_{vap}, ρ_{liq}, and ρ_{SC} in the homogeneous vapor and liquid phases as well as in the supercritical region.

According to Figure 3, the SRK EoS yields the best calculation results for p_{sat} and $\rho_{sat,vap}$ (slightly better than the YFR EoS) but at the cost of the worst calculations of liquid densities ρ_{liq} and $\rho_{sat,liq}$. Second to the YFR EoS, the PTV EoS yields the best calculations of the liquid densities ρ_{liq} and $\rho_{sat,liq}$, but obtains the worst result in the p_{sat} and $\rho_{sat,vap}$ calculations; this is exactly opposite to the SRK EoS. The PR EoS does not stand out or is not the worst for any properties. The performances of SRK, PR and PTV EoS observed in this work generally agree with the literature [4].

The YFR and PTV EoS were both developed based on the PT EoS and yielded improved liquid density calculations compared to the most commonly used PR and SRK EoS. A detailed comparison between YFR and PTV EoS is given in Figure 4, with methane taken as an example and REFPROP 10.0 for comparison. The relative deviation of p_{sat} and $\rho_{sat,vap}$ for both EoS are almost overlapping, which is the same for all other fluids. With the YFR EoS, the relative

deviations of most properties are generally smaller than the PTV EoS. However, the YFR EoS does not always improve the calculation, e.g., one observation is that at high pressures (e.g., p > 25 MPa) and temperatures near the T_C, the ρ_{SC} deviations are partly larger.

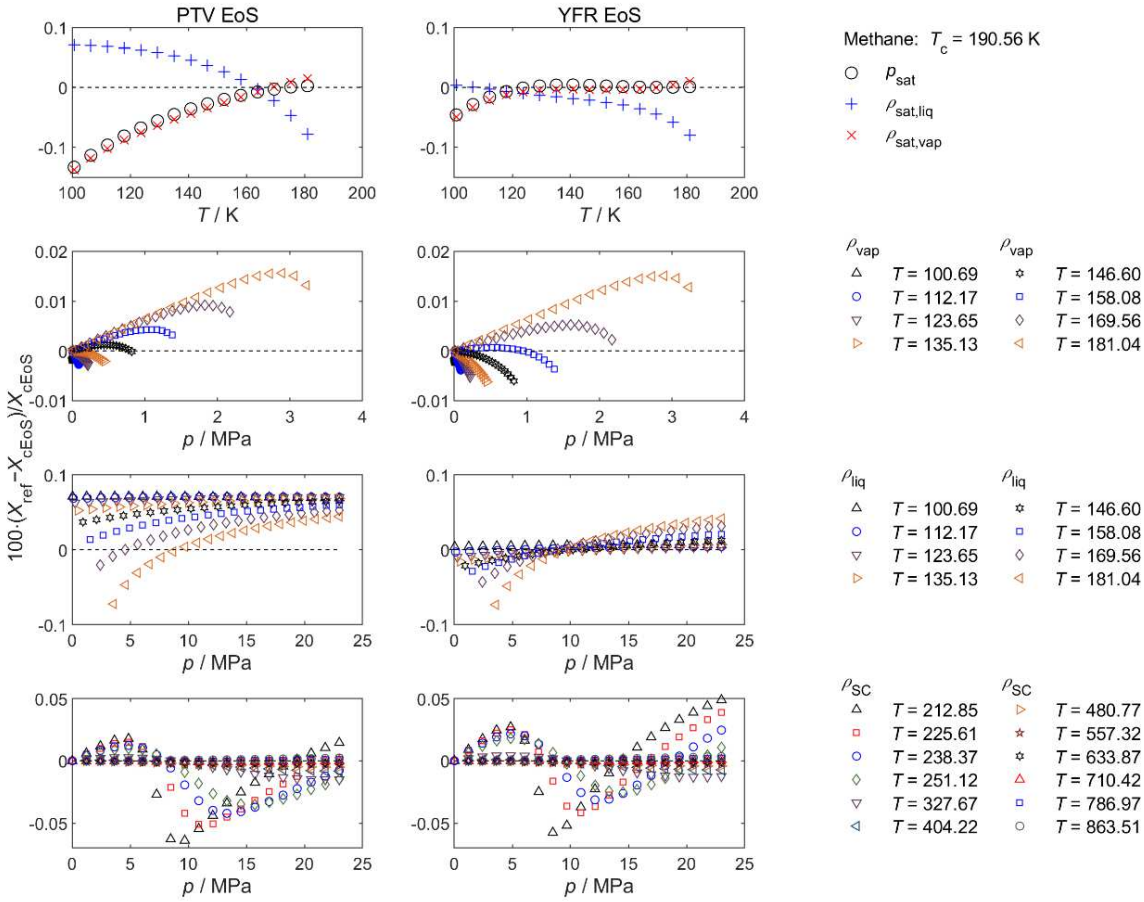

Figure 4. Relative deviations of properties of methane calculated with REFPROP 10.0 from values calculated with the PTV (left column) and YFR (right column) EoS . The properties are pressure p_{sat}, vapor density $\rho_{sat,vap}$, and liquid density $\rho_{sat,liq}$ at saturation conditions, and densities ρ_{vap}, ρ_{liq}, and ρ_{SC} in the homogeneous vapor and liquid phases as well as in the supercritical region.

4.2 Caloric Properties

With a cubic EoS, residual properties (difference between the real property and the ideal gas property at the same temperature and pressure) can be calculated. To evaluate the performance of the YFR EoS in the calculation of caloric properties (heat capacity, enthalpy, entropy and speed of

sound etc.), the ideal gas properties should be calculated with a proper method. In this work, we chose the simplest formation of ideal gas isobaric heat capacity c_p^0, i.e., c_p^0 as a linear function of temperature:

$$c_p^0 = k_1 \frac{(T - T_0)}{T_c} + k_0 \tag{17}$$

where k_0 is the value of c_p^0 at T_0 = 298.15 K, and k_1/T_c is the gradient of c_p^0 at T_0. The values of k_0 and k_1 for each pure fluid were obtained by fitting to values calculated with REFPROP 10.0 and have been implemented into our OilMixProp 1.0 software package [38]. The ideal gas property of other caloric properties can be derived from Eq. (17) according to their fundentmatal thermodynamic relations (e.g., see SI in [39]). The AARD of isobaric heat capacity c_p and speed of sound w calculated with the PR, SRK, PTV, and YFR EoS from reference values (calculated with REFPROP 10.0) in the homogeneous vapor and liquid phases as well as in the supercritical region are depicted in Figure 5, and similar results for entropy increment Δs and enthalpy increment Δh are shown in Figure 6. The YFR EoS shows a performance similar to other cubic EoS for most properties, except that slightly better results in Δs_{liq} and Δh_{liq} in the liquid phase but worse results in w_{liq} in the liquid phase were observed. Since all of the studied cubic EoS yield deviations higher than 15% in w_{liq}, we recommend not using cubic EoS for speed of sound calculations in the homogeneous liquid phase.

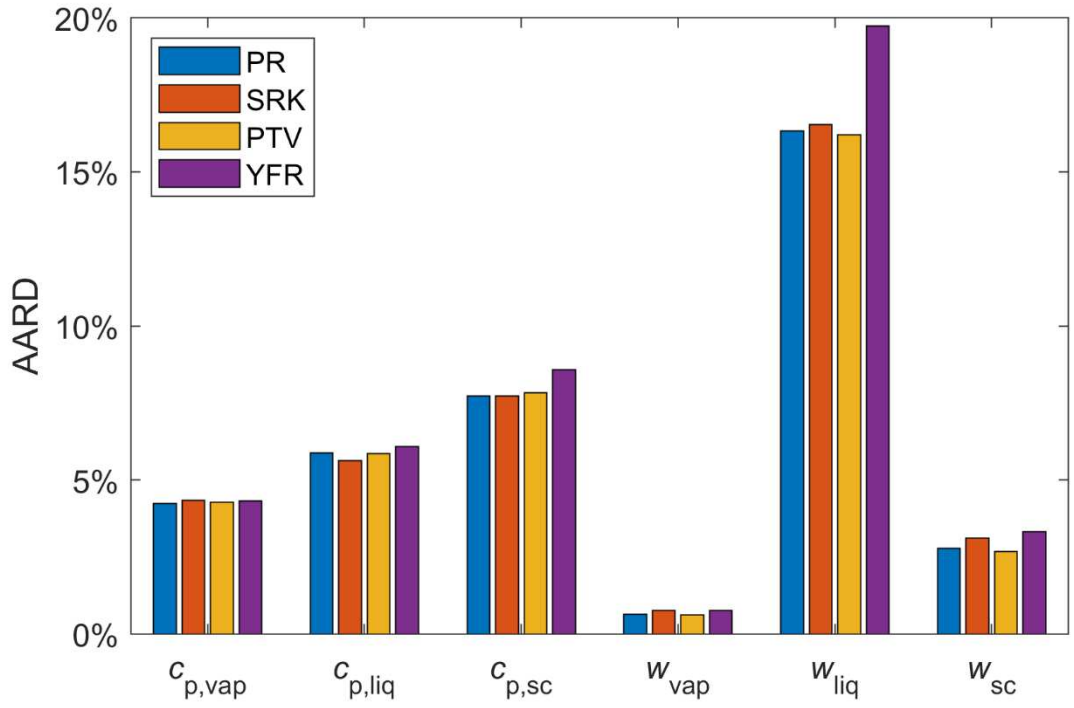

Figure 5. Relative deviations of isobaric heat capacity c_p and speed of sound w calculated with PR, SRK, PTV and YFR EoS from reference values (calculated with REFPROP 10.0). The subscripts 'vap', 'liq', and 'SC' refer to calculations in the homogeneous vapor and liquid phases as well as in the supercritical region.

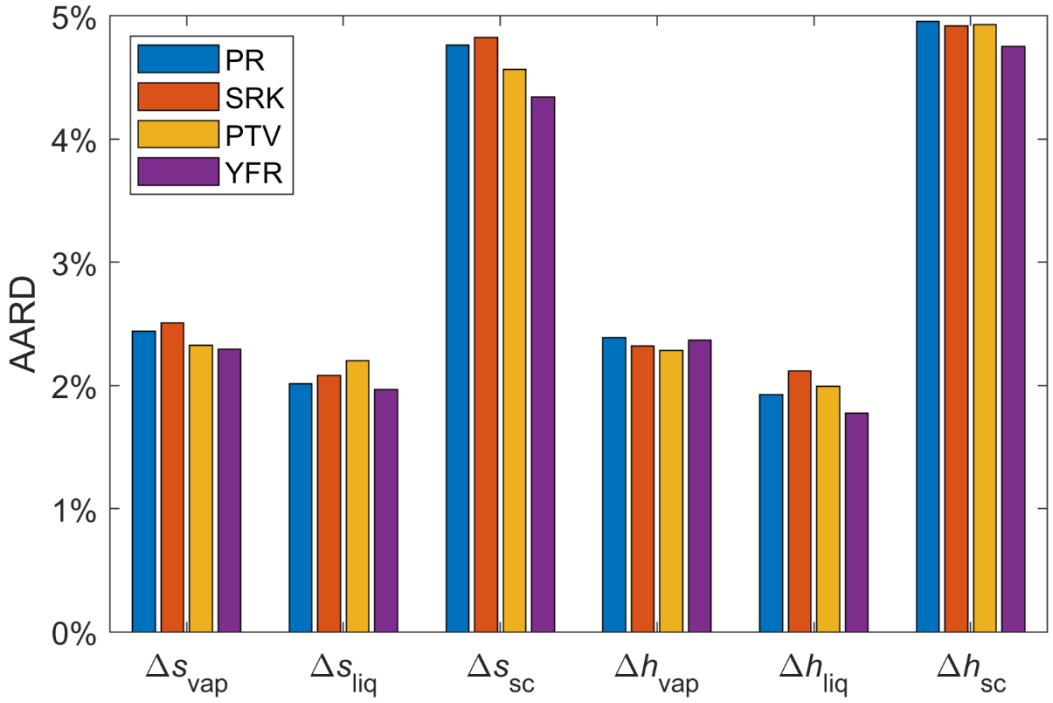

Figure 6. Relative deviations of entropy increment Δs and enthalpy increment Δh calculated with PR, SRK, PTV and YFR EoS from the reference values (calculated with REFPROP 10.0). The subscripts 'vap', 'liq', and 'SC' refer to calculations in the homogeneous vapor and liquid phases as well as in the supercritical region.

4.3 Thermodynamic Inconsistency

As mentioned above and discussed in the literature [24–27], the parameter b being temperature dependent yields thermodynamic inconsistency at high pressures. This subsection will study these inconsistencies and determine the application range of the YFR EoS.

4.3.1 Performance at High Temperatures and Pressures

The performance of the YFR EoS at extreme conditions, i.e., very high temperature and very high pressure, was investigated. First, the scenario of which Eq. (9) is not implemented was studied. For the calculations of density, heat capacity, enthalpy increment, entropy increment, and speed of sound of ethane (a randomly picked example), the relative deviations of four cubic EoS (PR, SRK, PTV, and YFR) from REFOROP 10.0 are plotted in Figure 7 at a pressure of 0.1 MPa with temperatures up to 1000 K, and in Figure 8 at a temperature of 305 K with pressures up to 150 MPa. As shown in Figure 7, in the whole temperature range, the YFR EoS shows almost a similar performance as other cubic EoS. However, except for density, the calculation of the YFR EoS clearly deviates from other EoS at high pressures, as can be seen in Figure 8.

To avoid such a defect at high pressures, considering that the YFR EoS is a semi-empirical EoS, we introduced Eq. (9), that is, the temperature derivatives of Ω_a, Ω_b and Ω_c are set to zero. Figures similar to those of Figure 7 and Figure 8 were plotted, and Figure 7 remained almost unchanged, i.e., the result at very high temperature was almost the same. However, the result at extremely high pressure was obviously improved, as can be seen in Figure 9. Calculating entropy is of particular interest, as its precision will be important in modeling transport properties (mainly viscosity and thermal conductivity) using residual entropy scaling approaches [12–14]. As a result, the entropy calculation with Eq. (9) is at a reasonable accuracy, which cannot be obtained without Eq. (9).

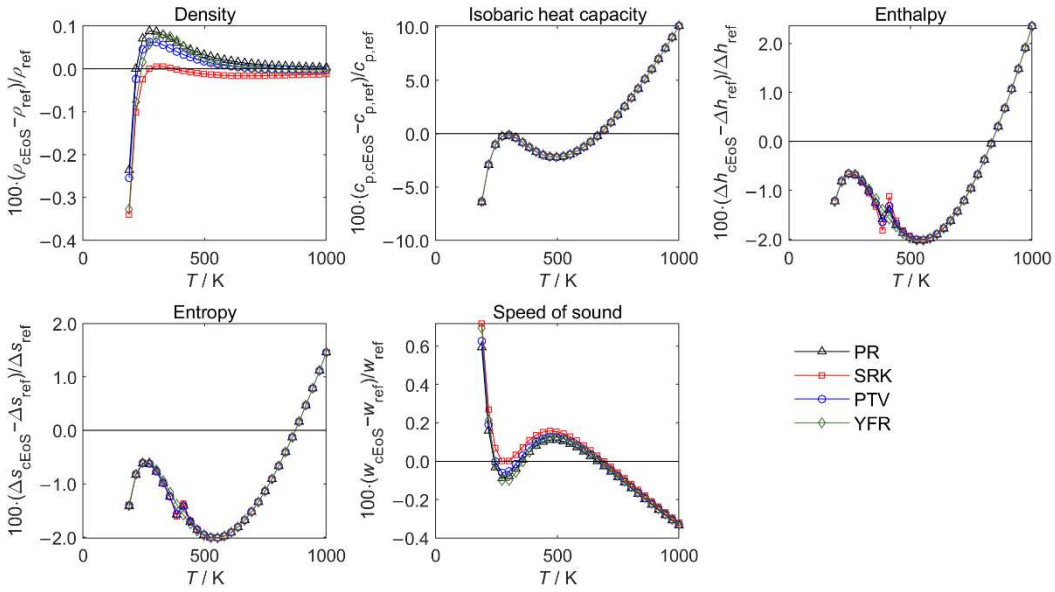

Figure 7. Relative deviations of four cubic EoS (PR, SRK, PTV and YFR) from REFOROP 10.0. The calculated properties are density, heat capacity, enthalpy increment, entropy increment, and

speed of sound of ethane at a pressure of 0.1 MPa. This figure is calculated without the simplification equation Eq. (9); we note that this figure remains almost unchanged with Eq. (9).

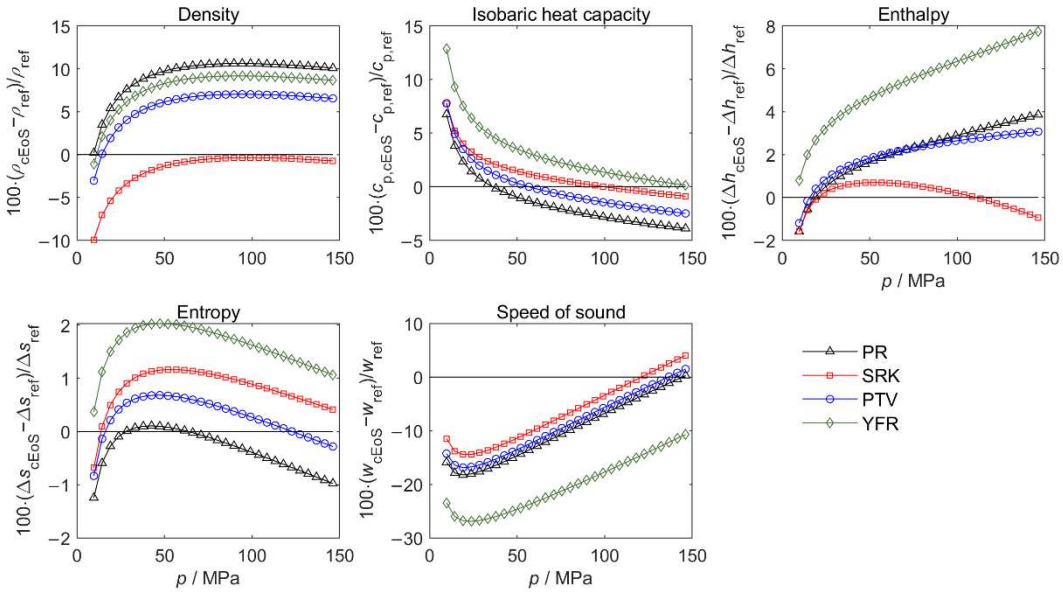

Figure 8. Relative deviations of four cubic EoS (PR, SRK, PTV, and YFR) from REFOROP 10.0. The calculated properties are density, heat capacity, enthalpy increment, entropy increment, and speed of sound of ethane at a temperature of 305 K. This figure is calculated <u>without</u> the simplification equation Eq. (9).

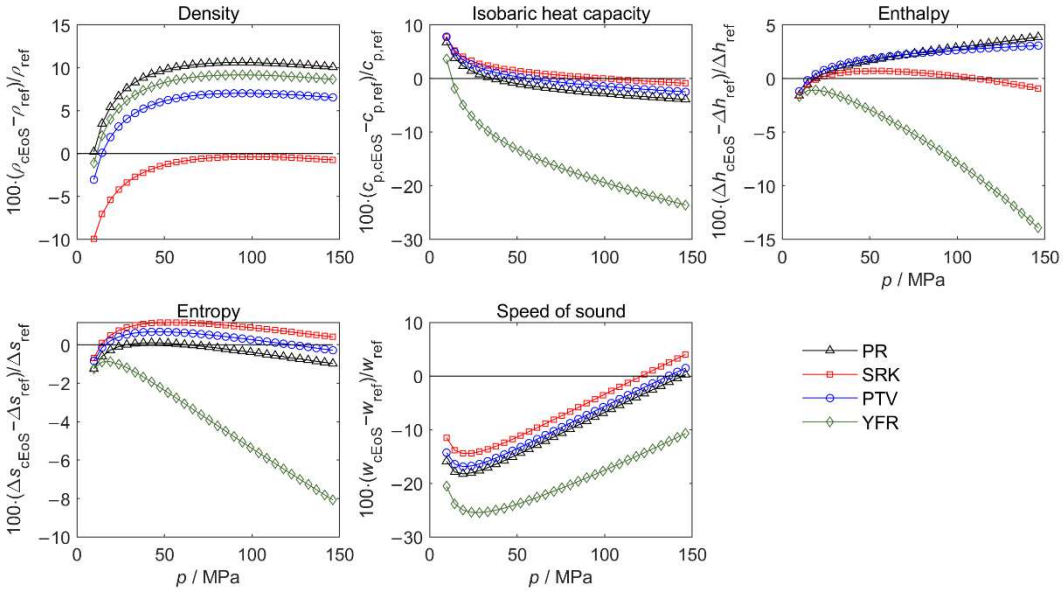

Figure 9. Relative deviations of four cubic EoS (PR, SRK, PTV, and YFR) from REFOROP 10.0. The calculated properties are density, heat capacity, enthalpy increment, entropy increment, and speed of sound of ethane at a temperature of 305 K. This figure is calculated with the simplification equation Eq. (9).

4.3.2 Selected Phase Diagrams

Parameter b in a cubic EoS being temperature dependent yields thermodynamic inconsistency at high pressures [24–27]. This inconsistency can be characterized by negative heat capacity values and crossing isotherms in the pressure vs. volume (p-v) phase diagram. The p-v, isobaric heat capacity vs. pressure (c_p-p), and isochoric heat capacity vs. pressure (c_v-p) phase diagrams of CO_2 (a randomly picked example) calculated with the YFR EoS from triple point temperature up to $3 \cdot T_c$ with pressures up to $100 \cdot p_c$ (730 MPa) are presented in Figure 10, Figure 11, and Figure 12, respectively. As shown in Figure 10, the isotherms are thermodynamically consistent except at pressures higher than approximately 200 MPa: some isotherms cross each other. Mainly because of the introduction of Eq. (9), there are no negative heat capacities observed in c_p-p and c_v-p phase diagrams, and according to Figure 11 and Figure 12, the heat capacities are not expected to become negative if the pressure increases further. With similar phase diagrams of some other fluids (e.g., those with low critical pressures) and considering that calculated values might already become inaccurate before the isotherms in the p-v phase diagram cross each other, we assume that the YFR EoS is still reliable at pressures below 100 MPa, and this is the application range of the YFR EoS.

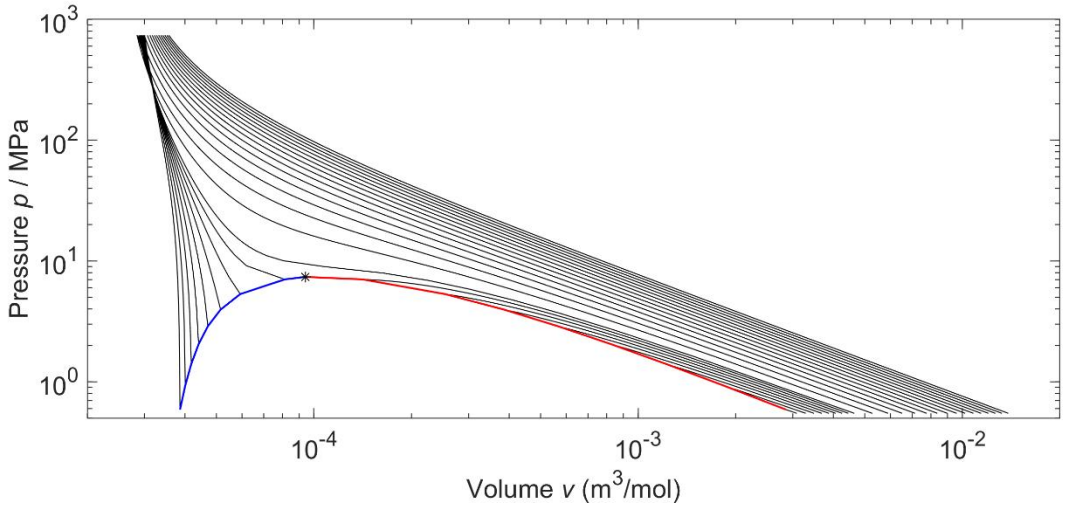

Figure 10. Pressure-volume phase diagram of CO_2 calculated with the YFR EoS. The blue curve is saturated liquid line, the red curve is saturated vapor line, and the black curves are isotherms from triple point temperature to three times the critical temperature.

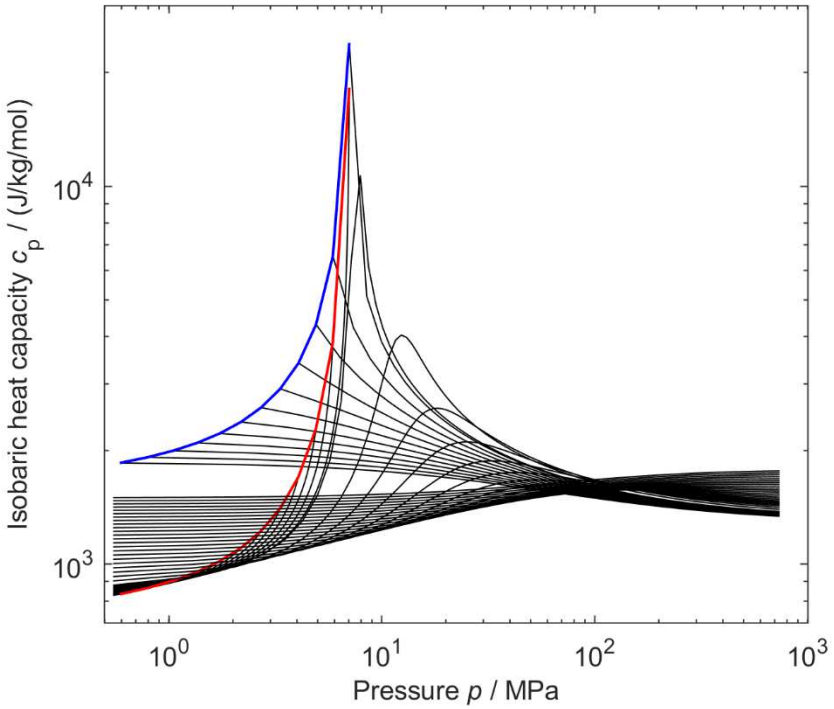

Figure 11. Isobaric heat capacity vs. pressure phase diagram of CO_2 calculated with the YFR EoS. The blue curve is saturated liquid line, the red curve is saturated vapor line, and the black curves are isotherms from triple point temperature to three times the critical temperature.

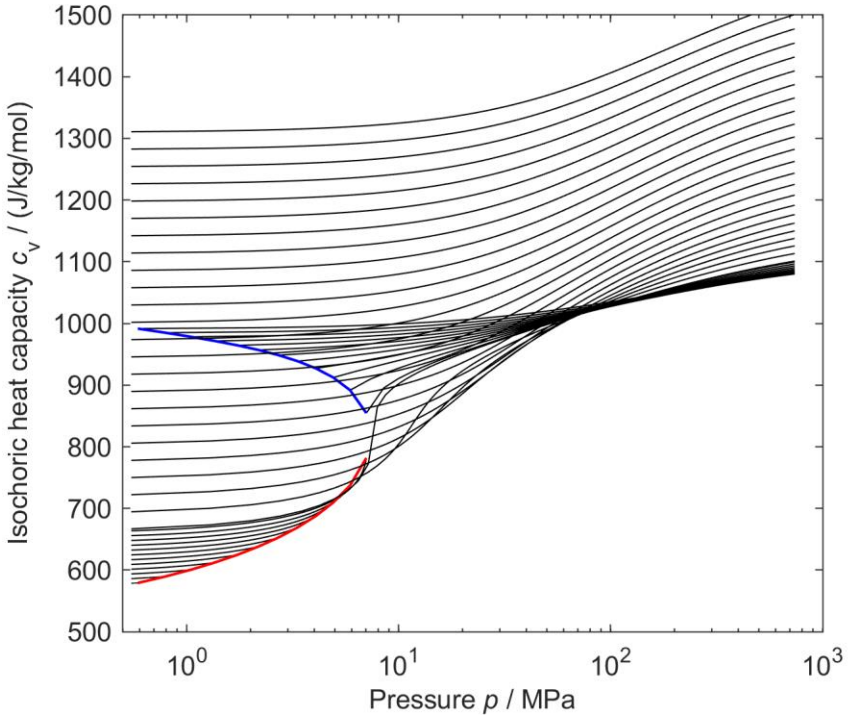

Figure 12. Isochoric heat capacity vs. pressure phase diagram of CO_2 calculated with the YFR EoS. The blue curve is saturated liquid line, the red curve is saturated vapor line, and the black curves are isotherms from triple point temperature to three times the critical temperature.

4.4 Application to Oils

To evaluate the YFR EoS in oil density calculation, (T, p, ρ) data of two oils, di-isodecyl phthalate (DIDP) and pentaerythritol tetra(2-ethylhexanoate) (PEB8), were collected from Peleties et al. [40] and Fandiño et al. [41], respectively. Three experimental (T, p, ρ) points at $p = 0.1$ MPa, as indicated by red dots in Figure 13, were used to fit the oils' constants using the method developed in our previous work [10] with both the PTV and YFR EoS. Note that PR and SRK EoS were not studied here because both cannot be used for fitting ω [10]. The fitted results are listed in Table 2. Here, $Z_c = 0.2563$ was recommended for the PTV EoS for oils, as discussed in our previous work, and $Z_c = 0.2640$ was recommended for the YFR EoS. These Z_c values are determined by trial and error, which is subject to future improvement.

Table 2. Parameters [a] fitted using the method described in our previous work [10]

Oil	EoS	M/(g·mol^{-1})	Z_c	T_c/K	ρ_c/(kg·m^{-3})	p_c/MPa	ω

DIDP	PTV	446.672	0.2563	778.326	294.226	1.0925	0.7772
DIDP	this work	446.672	0.2640	767.699	302.779	1.1423	0.6302
PEB8	PTV	640.900	0.2563	765.071	293.846	0.7475	0.9544
PEB8	this work	640.900	0.2640	754.047	302.434	0.7810	0.7054

[a] Parameters: molar mass M, the compressibility factor at the critical point Z_c, critical temperature T_c, critical density ρ_c, critical pressure p_c, and acentric factor ω.

Relative deviations of all the experimental (T, p, ρ) data of DIDP [40] and PEB8 [41] from both EoS predictions are shown in Figure 13. According to this figure, the YFR EoS represents the data generally within 3% and 2% for DIDP and PEB8, respectively. This is excessively good considering that the density was measured up to 140.0 MPa for DIDP and 60 MPa for PEB8, while the parameters were fitted only to data at ambient pressure. This is also a significant improvement compared to the PTV EoS, which shows deviations of up to 5% for DIDP.

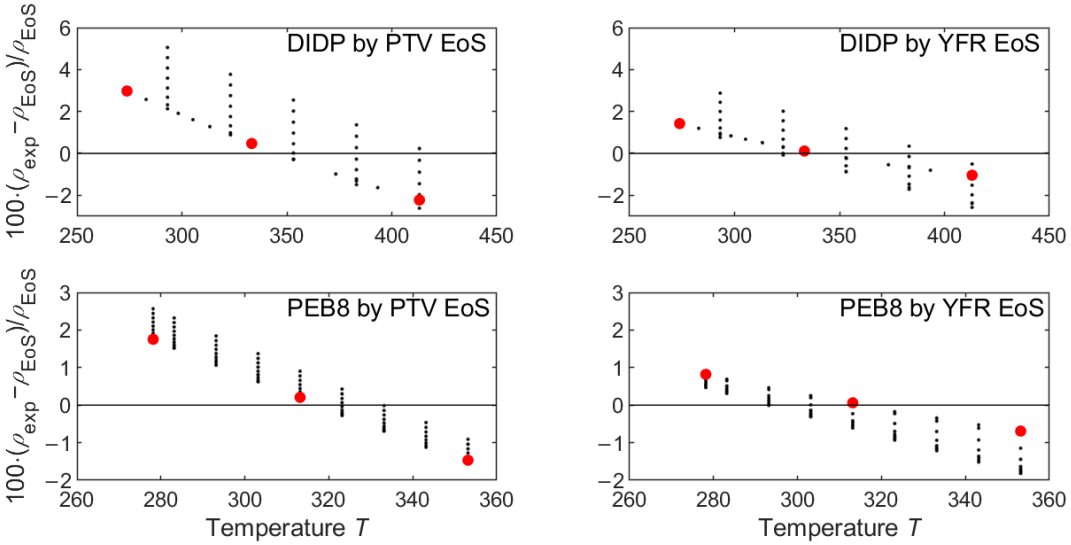

Figure 13. Relative deviations of the experimental density ρ_{exp} of DIDP [40] and PEB8 [41] from the values ρ_{EoS} calculated with the PTV and YFR EoS at $p = 0.1$ MPa. Red dots: data used for fitting fluid constants; small black dots: remaining experimental data.

5. Conclusions

In this work, a new general cubic equation of state (EoS) with improved accuracy in the liquid phase density calculation was developed using symbolic regression (SR) tools. The new cubic EoS, named YFR (Yang- Frotscher-Richter) EoS, was based on the functional form of Patel-Teja (PT) EoS [$p = RT/(v-b)–a/(v(v+b)+c(v-b)$], in which b and c are related to an empirical critical

compressibility factor ξ_C, and all these three parameters are constants for a pure fluid. In the YFR EoS, ξ_C, b and c are functions of temperature, and the corresponding equations were obtained by SR. This is the key to improving the accuracy of the liquid phase density but at the cost of increasing the complexity and thermodynamic inconsistency at high pressures (e.g., p > 100 MPa). A comprehensive study on thermodynamic inconsistency of the YFR EoS reveals that it is still very reliable at pressures below 100 MPa, and this is the application range of the EoS. The YFR EoS has been implemented in the OilMixProp 1.0 software package. Calculations of density (T, p, ρ) and phase equilibrium (T, p_{sat}, ρ_{sat}) of pure fluids with REFPROP 10.0 served as reference data for development, and almost all pure fluids in REFPROP 10.0 are studied. As a result, the average of the absolute value of relative deviations (AARD) of the YFR EoS from the calculated reference data are generally less than 3.0%. In particular, for liquid phase density, the AARD is as small as 2%, which is a clear improvement compared to 3% when using the Patel-Teja-Valderrama (PTV) EoS and 6% with the Peng-Robinson (PR) EoS.

Further evaluations of the YFR EoS were performed for the calculation of caloric properties. The ideal gas isobaric heat capacity was described by a linear function of temperature for the sake of calculating the ideal gas properties. The YFR EoS yields performance almost similar to that of other studied cubic EoS except for obtaining better results for isobaric heat capacity in the liquid phase but worse results in liquid phase speed of sound. More evaluations of transport properties will be presented in a future paper. The YFR EoS was also evaluated for density calculations of oils. It used three points of experimental liquid density at ambient pressure to fit the fluid constants of DIDP and PEB8, and its prediction agree with experimental data within 3% for DIDP up to 140.0 MPa and 2% for PEB8 up to 60 MPa. This is a significant improvement compared to the PTV EoS, which shows relative deviations of up to 5% from the experimental DIDP data.

Appendix: derivatives of the YFR EoS

To facilitate the application of the YFR EoS and if the simplification Eq. (9) is not implemented, a few important equations are presented here. The EoS can be reformulated as:

$$p = \frac{RT}{v-b} - \frac{a}{2d}\left(\frac{1}{v+m} - \frac{1}{v+q}\right) \tag{18}$$

Here

$$d = \left[bc + \frac{(b+c)^2}{4}\right]^{1/2}, \quad q = \frac{b+c}{2} + d, \quad m = \frac{b+c}{2} - d \tag{19}$$

The derivatives of d, q, m with respect to T are:

$$\frac{\mathrm{d}d}{\mathrm{d}T} = \frac{\frac{(b+c)}{2}\left(\frac{\mathrm{d}b}{\mathrm{d}T}+\frac{\mathrm{d}c}{\mathrm{d}T}\right)+b\frac{\mathrm{d}c}{\mathrm{d}T}+c\frac{\mathrm{d}b}{\mathrm{d}T}}{2\left(bc+\frac{(b+c)^2}{4}\right)^{1/2}}, \quad \frac{\mathrm{d}q}{\mathrm{d}T} = \frac{1}{2}\left(\frac{\mathrm{d}b}{\mathrm{d}T} + \frac{\mathrm{d}c}{\mathrm{d}T}\right) + \frac{\mathrm{d}d}{\mathrm{d}T}, \quad \frac{\mathrm{d}m}{\mathrm{d}T} = \frac{1}{2}\left(\frac{\mathrm{d}b}{\mathrm{d}T} + \frac{\mathrm{d}c}{\mathrm{d}T}\right) - \frac{\mathrm{d}d}{\mathrm{d}T} \tag{20}$$

$$\frac{\mathrm{d}^2d}{\mathrm{d}^2T} = \frac{\frac{(b+c)}{2}\left(\frac{\mathrm{d}^2b}{\mathrm{d}^2T}+\frac{\mathrm{d}^2c}{\mathrm{d}^2T}\right)+\frac{1}{2}\left(\frac{\mathrm{d}b}{\mathrm{d}T}+\frac{\mathrm{d}c}{\mathrm{d}T}\right)^2+b\frac{\mathrm{d}^2c}{\mathrm{d}^2T}+c\frac{\mathrm{d}^2b}{\mathrm{d}^2T}+2\frac{\mathrm{d}b}{\mathrm{d}T}\frac{\mathrm{d}c}{\mathrm{d}T}}{2\left(bc+\frac{(b+c)^2}{4}\right)^{1/2}} - \frac{\left(\frac{(b+c)}{2}\left(\frac{\mathrm{d}b}{\mathrm{d}T}+\frac{\mathrm{d}c}{\mathrm{d}T}\right)+b\frac{\mathrm{d}c}{\mathrm{d}T}+c\frac{\mathrm{d}b}{\mathrm{d}T}\right)^2}{4\left(bc+\frac{(b+c)^2}{4}\right)^{3/2}} \tag{21}$$

$$\frac{\mathrm{d}^2q}{\mathrm{d}^2T} = \frac{1}{2}\left(\frac{\mathrm{d}^2b}{\mathrm{d}^2T} + \frac{\mathrm{d}^2c}{\mathrm{d}^2T}\right) + \frac{\mathrm{d}^2d}{\mathrm{d}^2T}, \quad \frac{\mathrm{d}^2m}{\mathrm{d}^2T} = \frac{1}{2}\left(\frac{\mathrm{d}^2b}{\mathrm{d}^2T} + \frac{\mathrm{d}^2c}{\mathrm{d}^2T}\right) - \frac{\mathrm{d}^2d}{\mathrm{d}^2T} \tag{22}$$

The derivatives of X ($X = \Omega_a$, Ω_b and ξ_c) with respect to T are:

$$\frac{\mathrm{d}X}{\mathrm{d}T} = -4 \cdot n_{X,1} \cdot T^3/T_c^4 \cdot \exp(-T_r^4) - 3 \cdot n_{X,2} \cdot T^2/T_c^3 \cdot \exp(-T_r^3) \tag{23}$$

$$\frac{\mathrm{d}^2X}{\mathrm{d}^2T} = 9 \cdot n_{X,2} \cdot \frac{T^4}{T_c^6} \cdot \exp(-T_r^3) - 12 \cdot n_{X,1} \cdot \frac{T^2}{T_c^4} \cdot \exp(-T_r^4) - 6 \cdot n_{X,2} \cdot \frac{T}{T_c^3} \cdot \exp(-T_r^3) + 16 \cdot n_{X,1} \cdot T^6/T_c^8 \cdot \exp(-T_r^4) \tag{24}$$

At constant volume:

$$\left(\frac{\partial p}{\partial T}\right)_v = \frac{R}{v-b} - \frac{1}{2d}\left(\frac{1}{v+m} - \frac{1}{v+q}\right)\frac{\mathrm{d}a}{\mathrm{d}T} + \frac{a}{2d}\left(\frac{1}{(v+m)^2}\frac{\mathrm{d}m}{\mathrm{d}T} - \frac{1}{(v+q)^2}\frac{\mathrm{d}q}{\mathrm{d}T}\right) + \frac{a}{2d^2}\frac{\mathrm{d}d}{\mathrm{d}T}\left(\frac{1}{v+m} - \frac{1}{v+q}\right) + \frac{RT}{(v-b)^2}\frac{\mathrm{d}b}{\mathrm{d}T} \tag{25}$$

The residual properties can be calculated with:

$$a^{\mathrm{r}} = -RT\ln\frac{v-b}{v} + \frac{a}{2d}\ln\frac{v+m}{v+q} \tag{26}$$

$$s^{\mathrm{r}} = R\ln\frac{v-b}{v} - \frac{1}{2d}\frac{\mathrm{d}a}{\mathrm{d}T}\ln\frac{v+m}{v+q} - RT\frac{\mathrm{d}b}{\mathrm{d}T}\frac{1}{v-b} + \frac{\mathrm{d}d}{\mathrm{d}T}\frac{a}{2d^2}\ln\frac{v+m}{v+q} - \frac{a}{2d}\frac{v+q}{v+m}\left(\frac{\mathrm{d}m}{\mathrm{d}T}\frac{1}{v+q} - \frac{\mathrm{d}q}{\mathrm{d}T}\frac{v+m}{(v+q)^2}\right) \tag{27}$$

$$h^{\mathrm{r}} = \frac{RTb}{v-b} - \frac{a}{2d}\left(\frac{1}{v+m} - \frac{1}{v+q}\right) + \frac{1}{2d}\left(a - T\frac{\mathrm{d}a}{\mathrm{d}T}\right)\ln\frac{v+m}{v+q} \tag{28}$$

$$c_v^{\mathrm{r}} = T\left(\frac{2R}{b-v}\frac{\mathrm{d}b}{\mathrm{d}T} - \frac{1}{2d}\frac{\mathrm{d}^2a}{\mathrm{d}^2T}\ln\frac{v+m}{v+q} - \frac{a}{2d}\left(-\frac{1}{(v+m)^2}\left(\frac{\mathrm{d}m}{\mathrm{d}T}\right)^2 + \frac{1}{(v+q)^2}\left(\frac{\mathrm{d}q}{\mathrm{d}T}\right)^2 + \frac{1}{v+m}\frac{\mathrm{d}^2m}{\mathrm{d}^2T} - \frac{1}{v+q}\frac{\mathrm{d}^2q}{\mathrm{d}^2T}\right) - \frac{1}{d}\frac{\mathrm{d}a}{\mathrm{d}T}\left(\frac{1}{v+m}\frac{\mathrm{d}m}{\mathrm{d}T} - \frac{1}{v+q}\frac{\mathrm{d}q}{\mathrm{d}T}\right) - \frac{a}{d^3}\left(\frac{\mathrm{d}d}{\mathrm{d}T}\right)^2\ln\frac{v+m}{v+q} + \frac{RT}{b-v}\frac{\mathrm{d}^2b}{\mathrm{d}^2T} + \frac{a}{d^2}\frac{\mathrm{d}d}{\mathrm{d}T}\left(\frac{1}{v+m}\frac{\mathrm{d}m}{\mathrm{d}T} - \frac{1}{v+q}\frac{\mathrm{d}q}{\mathrm{d}T}\right) - \frac{RT}{(b-v)^2}\left(\frac{\mathrm{d}b}{\mathrm{d}T}\right)^2 + \frac{1}{d^2}\frac{\mathrm{d}a}{\mathrm{d}T}\frac{\mathrm{d}d}{\mathrm{d}T}\ln\frac{v+m}{v+q} + \frac{a}{2d^2}\frac{\mathrm{d}^2d}{\mathrm{d}^2T}\ln\frac{v+m}{v+q}\right) \tag{29}$$

$$c_p^{\mathrm{r}} = c_v^{\mathrm{r}} - R - T\left(\frac{\partial p}{\partial T}\right)_v^2 \Big/ \left(\frac{\partial p}{\partial v}\right)_T \tag{30}$$

Other equations are generally the same as those used in the PTV EoS [1].

Acknowledgment

The authors are very thankful to Prof. J. P. Martin Trusler of Imperial College London and to Prof. Jean-Noël Jaubert of Université de Lorraine for valuable discussions and the provision of further literature.

Statements and Declarations

- Funding: The realization of the project and the scientific work was supported by the German Federal Ministry of Education and Research on the basis of a decision by the German Bundestag (funding code 03SF0623A). The authors gratefully acknowledge this support and carry full responsibility for the content of this paper. Moreover, part of this work was funded by the Deutsche Forschungsgemeinschaft (DFG, German Research Foundation) within the priority program SPP 2331, Project Number 466528284.
- Competing interests: The authors have no competing interests to declare that are relevant to the content of this paper.
- Ethics approval: The work contains no libelous or unlawful statements, does not infringe on the rights of others, or contains material or instructions that might cause harm or injury.
- Consent to participate: The authors consent to participate.
- Consent for publication: All authors read the final version of the manuscript and consent to publish.
- Code availability: Not applicable.
- Authors' contributions: Conceptualization: XY; Methodology: XY and OF; Software: XY; Validation: XY and MR; Formal Analysis: XY; Investigation: XY and OF; Resources: MR;

Data Curation: XY; Writing - Original Draft: XY; Writing - Review & Editing: OF and MR; Visualization: XY; Supervision: MR; Project Administration: MR; Funding Acquisition: MR.

Reference

1. J. O. Valderrama, Ind. Eng. Chem. Res. **42**, 1603 (2003).
2. W. Zhao, L. Xia, X. Sun, and S. Xiang, Int J Thermophys **40**, 105 (2019).
3. R. Privat and J.-N. Jaubert, Fluid Phase Equilib. **567**, 113697 (2023).
4. P. N. P. Ghoderao, M. Narayan, V. H. Dalvi, and H. S. Byun, Fluid Phase Equilib. **567**, 113707 (2023).
5. H. Sugie, Y. Iwahori, and B. C.-Y. Lu, Fluid Phase Equilib. **50**, 1 (1989).
6. E. W. Lemmon, I. H. Bell, M. L. Huber, and M. O. McLinden, *NIST Standard Reference Database 23: Reference Fluid Thermodynamic and Transport Properties-REFPROP, Version 10.0, National Institute of Standards and Technology* (2018).
7. R. Span, R. Beckmüller, S. Hielscher, A. Jäger, E. Mickoleit, T. Neumann, and S. Pohl, *TREND. Thermodynamic Reference and Engineering Data 5.0.* (Bochum, Germany: Lehrstuhl für Thermodynamik, Ruhr-Universität Bochum, 2020).
8. I. H. Bell, J. Wronski, S. Quoilin, and V. Lemort, Ind. Eng. Chem. Res. **53**, 2498 (2014).
9. N. C. Patel and A. S. Teja, Chem. Eng. Sci. **37**, 463 (1982).
10. X. Yang, C. Hanzelmann, S. Feja, J. M. Trusler, and M. Richter, Ind. Eng. Chem. Res. **62**, 18736 (2023).
11. X. Yang and M. Richter, "Thermophysical Property Model of Lubricant Oils and Their Mixtures with Refrigerants" in *2024 Herrick Conferences* (West Lafayette, IN, USA, 2024).
12. X. Yang, X. Xiao, E. F. May, and I. H. Bell, J. Chem. Eng. Data **66**, 1385 (2021).
13. X. Yang, D. Kim, E. F. May, and I. H. Bell, Ind. Eng. Chem. Res. **60**, 13052 (2021).
14. X. Yang, X. Xiao, M. Thol, M. Richter, and I. H. Bell, Int. J. Thermophys. **43**, 183 (2022).
15. X. Yang, X. Xiao, M. Thol, M. Richter, and I. Bell, "A Residual Entropy Scaling Approach for Viscosity of Refrigerants, other Fluids and their Mixtures" in (6th International Congress of Refrigeration| August 21st-25th, 2023| Paris …, 2023).
16. Z. Li, Y. Duan, and X. Yang, Ind. Eng. Chem. Res. **63**, 18160 (2024).
17. V. Martinek, X. Yang, I. H. Bell, R. Herzog, and M. Richter, J. Chem. Eng. Data (under review) (2024).
18. G. Soave, Chem. Eng. Sci. **27**, 1197 (1972).
19. D.-Y. Peng and D. B. Robinson, Ind. Eng. Chem. Fundam. **15**, 59 (1976).
20. R. Stryjek and J. H. Vera, Can. J. Chem. Eng. **64**, 323 (1986).
21. G. M. Wilson, "Vapor-liquid equilibria, correlation by means of a modified Redlich-Kwong equation of state" in *Advances in Cryogenic Engineering* (Springer, 1964), pp. 168–176.
22. J. O. Valderrama, J. Chem. Eng. Jpn. **23**, 87 (1990).
23. O. Redlich and J. N. S. Kwong, Chem. Rev. **44**, 233 (1949).
24. H. B. de Sant'Ana, P. Ungerer, and J. C. de Hemptinne, Fluid Phase Equilib. **154**, 193 (1999).
25. V. Kalikhman, D. Kost, and I. Polishuk, Fluid Phase Equilib. **293**, 164 (2010).
26. A. Piña-Martinez, R. Privat, S. Lasala, G. Soave, and J.-N. Jaubert, Fluid Phase Equilib. **522**, 112750 (2020).
27. J.-N. Jaubert, R. Privat, Y. Le Guennec, and L. Coniglio, Fluid Phase Equilib. **419**, 88 (2016).

28. S. Bair and W. O. Winer, J. Tribol. **114**, 1 (1992).
29. A. I. Vakis, V. A. Yastrebov, J. Scheibert, L. Nicola, D. Dini, C. Minfray, A. Almqvist, M. Paggi, S. Lee, G. Limbert, J. F. Molinari, G. Anciaux, R. Aghababaei, S. Echeverri Restrepo, A. Papangelo, A. Cammarata, P. Nicolini, C. Putignano, G. Carbone, S. Stupkiewicz, J. Lengiewicz, G. Costagliola, F. Bosia, R. Guarino, N. M. Pugno, M. H. Müser, and M. Ciavarella, Tribol. Int. **125**, 169 (2018).
30. V. Martinek, O. Frotscher, M. Richter, and R. Herzog, "Introducing Thermodynamics-Informed Symbolic Regression -- A Tool for Thermodynamic Equations of State Development" in (arXiv, 2023).
31. O. Frotscher, R. Herzog, and M. Richter, Int. J. Thermophys. **42**, 96 (2021).
32. L. D. Tenardi, O. Frotscher, X. Yang, F. Jiao, M. Richter, P. L. Stanwix, and E. F. May, Int. J. Thermophys. **44**, 14 (2022).
33. O. Frotscher, V. Martinek, R. Fingerhut, X. Yang, J. Vrabec, R. Herzog, and M. Richter, Int. J. Thermophys. **44**, 105 (2023).
34. M. Sekulla, L. Bernardini, S. Werth, M. Kohns, and M. Richter, Ind. Eng. Chem. Res. **63**, 16907 (2024).
35. V. Martinek, J. Reuter, O. Frotscher, S. Mostaghim, M. Richter, and R. Herzog, "Shape Constraints in Symbolic Regression using Penalized Least Squares" in (arXiv, 2024).
36. T. Urbaneck, M. Matthes, M. Richter, O. Hempel, M. Safarik, U. Franzke, R. Noack, M. Honke, M. Müller, S. Henninger, P. Schossig, H.-M. Henning, H. T. de Oliveira, A. Morgenstern, B. Nienborg, S. Gschwander, P. Engelmann, and G. Benndorf, "Research Platform Refrigeration and Energy Technology (KETEC)" in (2022).
37. X. Yang, D. Rowland, C. C. Sampson, P. E. Falloon, and E. F. May, Fuel **314**, 123033 (2022).
38. X. Yang and M. Richter, "OilMixProp 1.0: Package for Thermophysical Properties of Oils, Common Fluids, and Their Mixtures" in (IOP Publishing, Dortmund, 2024), p. (in press).
39. X. Yang, F. Yang, and F. Yang, Energy **272**, 127041 (2023).
40. F. Peleties, J. J. Segovia, J. P. M. Trusler, and D. Vega-Maza, J. Chem. Thermodyn. **42**, 631 (2010).
41. O. Fandiño, A. S. Pensado, L. Lugo, M. J. P. Comuñas, and J. Fernández, J. Chem. Eng. Data **50**, 939 (2005).